REVISTA INTERDISCIPLINAR DE PESQUISA EM ENGENHARIA

FINITE ELEMENT LIMIT ANALYSIS OF REINFORCED SOILS BY THE STATIC THEOREM

Eric L.B. Cavalcante

Eliseu Lucena Neto

Paulo I. B. de Queiroz

ericlb@ita.br

eliseu@ita.br

pi@ita.br

Instituto Tecnológico de Aeronáutica

Praça Marechal Eduardo Gomes, 50, 12228-900, SP, Brazil

Denilson J.R. Sodré

dsodre@ufpa.br

Universidade Federal do Pará

Rua Augusto Corrêa, 1, 66075-110, PA, Brazil

Abstract. *Two finite element formulations for the lower bound limit analysis of reinforced soil structures in plane strain are described. The material idealization is based on the idea that, from a macroscopic point of view, reinforced soil can be treated as a homogeneous material with anisotropic properties. The overall behavior of the reinforced soil is controlled by the mechanical properties of the soil and the reinforcement, as well as their relative proportions and geometrical arrangement. One element satisfies the equilibrium equation, for a constant body force, and the mechanical boundary condition, for prescribed traction with linearly distributed components, in a strict pointwise sense. The other element satisfies the equilibrium equation and the mechanical boundary condition only in a weak sense. The equilibrium equation, the mechanical boundary condition and the linearized yield criterion, expressed in terms of nodal stresses, are dealt with as constraints of a linear optimization problem whose objective function is defined by the loading. Examples are given to illustrate the effectiveness*

of the proposed procedures for computing lower bounds on the collapse load of reinforced soil structures.

Keywords: *Finite Element, Limit Analysis, Optimization, Reinforced soil*

1 INTRODUCTION

In the design process of geotechnical structures, it is necessary to determine the maximum load to be resisted at the impending collapse. The ability of the methods to accurately estimate ultimate limit states depends on the fulfillment of theoretical requirements derived from continuum mechanics concerning the equilibrium, strain-displacement relations, constitutive behavior and boundary conditions.

The increasing use of reinforced earth in geotechnical engineering requires the development of reliable and practical yield design methods for reinforced earth structures. Although comprehensive analytical and finite element studies of reinforced soil behavior are possible, they are inevitably complicated by the fact that the precise geometry of the reinforcement and the elastic-plastic nature of the soil needs to be fully taken into account (Yu & Sloan, 1997).

The limit theorems, which have proved to be a most effective means of predicting the plastic collapse of earth structures in many areas of soil mechanics, provide an alternative approach for studying the behavior of reinforced soil. We assume that on a macroscopic scale reinforced soil behaves as a homogeneous but anisotropic material, whose composite strength can be estimated from the strength characteristics of its components. The limit analysis procedures derived from this assumption have been successfully applied to predict the observed behavior of reinforced foundations and retaining walls in the past: Sawicki (1983, 1988); de Buhan *et al*. (1989); de Buhan & Siad (1989); Yu & Sloan (1997).

In this paper, specific attention is focused on the lower bound approach coupled with the finite element method to provide safe lower bound solutions for reinforced soil structures in plane strain. To begin the formulation, the conventional isotropic Mohr-Coulomb yield criterion is modified to include the effect of anisotropy which is caused by the presence of reinforcement. The influence of the soil-reinforcement failure conditions on the overall behavior is taken into account by assuming that the shear and normal stresses at the soil-reinforcement interface are governed by a general Mohr-Coulomb criterion. The numerical formulation of the static theorem using the modified anisotropic yield criterion is then developed. Using a suitable linear approximation of the yield surface, the application of the static theorem leads to a linear programming problem.

A balance between accuracy, efficiency, clarity of the formulation and simplicity distinguishes two three-node triangular finite elements to be used. The first one is the well-known element proposed by Lysmer (1970). The second one is the element found in Silva *et al.* (1999). The first can provide rigorous lower bound solutions and has been widely used, whereas the other has not yet attracted interest possibly for leading to solutions that are not strict lower bound.

2 FAILURE CONDITIONS FOR REINFORCED SOILS

The reinforced soil is treated as a homogeneous material with anisotropic properties. The reinforcement is assumed to be unidirectional with thickness d very small compared to the space h between two reinforcements ($d/h \ll 1$). Three stress tensors are defined at every point in the homogenized continuum (Fig. 1): the tensor $\boldsymbol{\sigma}^m = \lfloor \sigma_t \quad \sigma_n \quad \tau_{tn} \rfloor^T$ for macrostresses, and the tensors $\boldsymbol{\sigma}^s = \lfloor \sigma_t^s \quad \sigma_n^s \quad \tau_{tn}^s \rfloor^T$ and $\boldsymbol{\sigma}^r = \lfloor \sigma_t^r \quad \sigma_n^r \quad \tau_{tn}^r \rfloor^T$ for microstresses which act on the soil and reinforcement respectively (de Buhan *et al.*, 1989; Yu & Sloan, 1997). The tensor components are related by

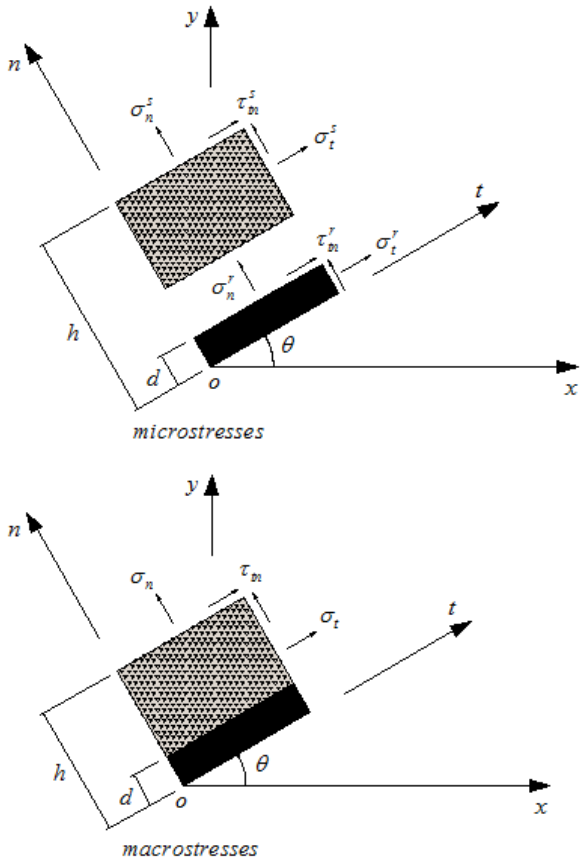

Figure 1. Stresses on reinforced soil

$$\begin{aligned}\sigma_t &= \sigma_t^s + \frac{d}{h}\sigma_t^r = \sigma_t^s + \sigma^r \\ \sigma_n &= \sigma_n^s = \sigma_n^r \\ \tau_{tn} &= \tau_{tn}^s = \tau_{tn}^r\end{aligned} \tag{1}$$

where $\sigma^r = d/h\,\sigma_t^r$.

The macrostress components in the orthogonal Cartesian coordinate systems xy e tn are related by

$$\begin{aligned}\sigma_x &= \sigma_t \cos^2\theta + \sigma_n \sin^2\theta - 2\tau_{tn}\sin\theta\cos\theta \\ \sigma_y &= \sigma_t \sin^2\theta + \sigma_n \cos^2\theta + 2\tau_{tn}\sin\theta\cos\theta \\ \tau_{xy} &= (\sigma_t - \sigma_n)\sin\theta\cos\theta + \tau_{tn}(\cos^2\theta - \sin^2\theta)\end{aligned} \tag{2}$$

where θ represents the angle between the horizontal axis x and the reinforcement direction t, measured counterclockwise. Substitution of Eqs. (1) and relations

$$\begin{aligned}\sigma_t^s &= \sigma_x^s \cos^2\theta + \sigma_y^s \sin^2\theta + 2\tau_{xy}^s \sin\theta\cos\theta \\ \sigma_n^s &= \sigma_x^s \sin^2\theta + \sigma_y^s \cos^2\theta - 2\tau_{xy}^s \sin\theta\cos\theta \\ \tau_{tn}^s &= -\left(\sigma_x^s - \sigma_y^s\right)\sin\theta\cos\theta + \tau_{xy}^s(\cos^2\theta - \sin^2\theta)\end{aligned} \tag{3}$$

into Eqs. (2) yields

$$\sigma_x^s = \sigma_x - \sigma^r \cos^2\theta$$
$$\sigma_y^s = \sigma_y - \sigma^r \sin^2\theta$$
$$\tau_{xy}^s = \tau_{xy} - \sigma^r \sin\theta\cos\theta. \quad (4)$$

The reinforcement inside the soil is supposed to act merely as tensile load carrying elements, and offer no resistance to shear, bending or compression. The constraint $0 \le \sigma^r \le \sigma_o$ is therefore imposed on σ^r, where $\sigma_o = (d/h)\sigma_{yield}$ is the tensile yield strength σ_{yield} of the reinforcement times the volume fraction of the reinforcement.

The soil mass with cohesion c and angle of internal friction ϕ is assumed to obey the Mohr-Coulomb yield criterion in plane strain condition and may be expressed as

$$F_s = \left(\sigma_x^s - \sigma_y^s\right)^2 + \left(2\tau_{xy}^s\right)^2 - \left[2c\cos\phi - \left(\sigma_x^s + \sigma_y^s\right)\sin\phi\right]^2 = 0. \quad (5)$$

This can be written in terms of the macrostresses and σ^r by using Eqs. (4) to give

$$F_s = \left(\sigma_x - \sigma_y - \sigma^r\cos 2\theta\right)^2 + \left(2\tau_{xy} - \sigma^r \sin 2\theta\right)^2 - \left[2c\cos\phi - \left(\sigma_x + \sigma_y - \sigma^r\right)\sin\phi\right]^2 = 0. \quad (6)$$

The soil-reinforcement interface failure condition is expressed as

$$F_i = |\tau_{tn}| - c_i + \sigma_n \tan\phi_i = 0 \quad (7)$$

where τ_{tn} is the shear stress, σ_n is the normal stress, and c_i and ϕ_i denote the interface cohesion and interface friction angle, respectively. The above failure criterion can be expressed in terms of the macrostress tensor using the inverse of Eqs. (2) (Eq. (3) without superscript s) to give:

$$F_i = \frac{1}{2}\left|\left(\sigma_y - \sigma_x\right)\sin 2\theta + 2\tau_{xy}\cos 2\theta\right| - c_i + \left(\sigma_x \sin^2\theta + \sigma_y\cos^2\theta - \tau_{xy}\sin 2\theta\right)\tan\phi_i = 0. \quad (8)$$

3 STATIC THEOREM

The limit analysis relies on the assumption of an elastic-perfectly plastic material with a flow rule associated to a convex yield surface, and also on small displacement gradients so that the solid does not undergo large deformation at collapse. The lower bound approach follows the static theorem, which requires that the assumed stress field must satisfy the equilibrium equation, the mechanical boundary condition and the yield criterion everywhere. Under these idealized conditions, the computed limit load is a lower bound on the true collapse load (Chen, 1975).

3.1 Equilibrium equation

Let Ω be the region occupied by the reinforced soil subjected to the body force $\boldsymbol{b} = \lfloor b_x \quad b_y \rfloor^T$ expressed in the orthogonal Cartesian coordinate system xy. The macrostress $\boldsymbol{\sigma} = \lfloor \sigma_x \quad \sigma_y \quad \tau_{xy} \rfloor^T$ must satisfy the equilibrium equation

$$\boldsymbol{D\sigma} + \boldsymbol{b} = \boldsymbol{0} \quad (9)$$

throughout the domain Ω, where the differential operator

$$\boldsymbol{D} = \begin{bmatrix} \frac{\partial}{\partial x} & 0 & \frac{\partial}{\partial y} \\ 0 & \frac{\partial}{\partial y} & \frac{\partial}{\partial x} \end{bmatrix}. \tag{10}$$

3.2 Mechanical boundary condition

Let Γ be the boundary of the domain Ω, with unit outward normal vector denoted by $\boldsymbol{n} = \lfloor n_x \quad n_y \rfloor^T$. In addition to Eq. (9), the stress field must also satisfy the mechanical boundary condition

$$\boldsymbol{t} = \boldsymbol{N}\boldsymbol{\sigma} = \bar{\boldsymbol{t}} \tag{11}$$

on the portion Γ_t of Γ on which the traction (stress vector) $\boldsymbol{t} = \lfloor t_x \quad t_y \rfloor^T$ is prescribed as being $\bar{\boldsymbol{t}}$. Matrix

$$\boldsymbol{N} = \begin{bmatrix} n_x & 0 & n_y \\ 0 & n_y & n_x \end{bmatrix} \tag{12}$$

contains the components of $\boldsymbol{n}$.

3.3 Yield criteria

To assure that the yield conditions are satisfied it is necessary to impose

$$F_s \leq 0 \qquad F_i \leq 0 \qquad 0 \leq \sigma^r \leq \sigma_o. \tag{13}$$

From Eq. (8), it is readily seen that the second of Eqs. (13) results in two linear constraints on the macrostresses. In order to carry out the analysis as a linear programming problem, the first of Eqs. (13) should be linearized as described next.

To proceed with an approximated piecewise linearization of the first of Eqs. (13), the change of variables

$$\begin{aligned} X &= \sigma_x - \sigma_y - \sigma^r \cos 2\theta \\ Y &= 2\tau_{xy} - \sigma^r \sin 2\theta \\ R &= 2c \cos\phi - \left(\sigma_x + \sigma_y - \sigma^r\right) \sin\phi \end{aligned} \tag{14}$$

is introduced so that $F_s = 0$ becomes the circumference

$$X^2 + Y^2 = R^2 \tag{15}$$

of radius R in the XY-space. The circumference is then approximated by an inscribed regular polygon of p sides and p vertices, as shown in Fig. 2.

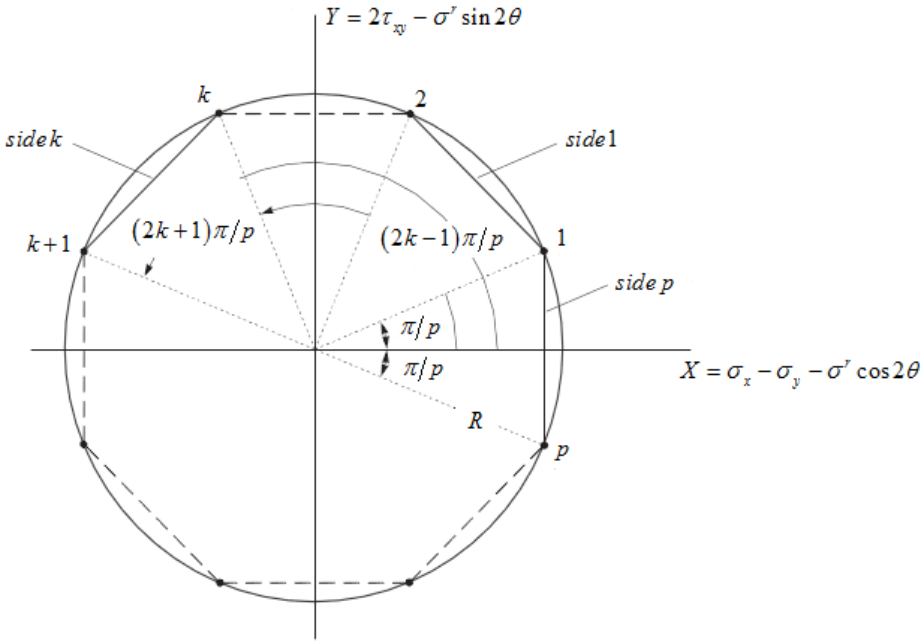

Figure 2. Circumference approximated by an inscribed regular polygon of p sides in the representation of the yield condition $F_s \leq 0$

The first vertex is defined by the angle π/p rad measured counterclockwise from the X-axis by constraining the last side p to be perpendicular to the X-axis. The X and Y coordinates of two consecutives vertices k and $k + 1$ are

$$X_k = R\cos(2k-1)\frac{\pi}{p} \qquad Y_k = R\sin(2k-1)\frac{\pi}{p}$$
$$X_{k+1} = R\cos(2k+1)\frac{\pi}{p} \qquad Y_{k+1} = R\sin(2k+1)\frac{\pi}{p}. \tag{16}$$

The side k, between vertices k and $k + 1$, has the equation

$$(Y_k - Y_{k+1})X + (X_{k+1} - X_k)Y + X_kY_{k+1} - X_{k+1}Y_k = 0 \qquad k = 1,2,\dots,p. \tag{17}$$

The linearized form of the yield criterion is then provided substituting Eqs. (14) and Eqs. (16) into Eq. (17):

$$F_s = A_k\sigma_x + B_k\sigma_y + C_k\tau_{xy} - D_k\sigma^r - 2c\cos\phi\cos\frac{\pi}{p} \qquad k = 1,2,\dots,p \tag{18}$$

where

$$A_k = \cos\frac{2k\pi}{p} + \sin\phi\cos\frac{\pi}{p} \quad B_k = \sin\phi\cos\frac{\pi}{p} - \cos\frac{2k\pi}{p}$$
$$C_k = 2\sin\frac{2k\pi}{p} \qquad D_k = \cos 2\theta\cos\frac{2k\pi}{p} + \sin 2\theta\sin\frac{2k\pi}{p} + \sin\phi\cos\frac{\pi}{\rho}. \tag{19}$$

It is clear from Fig. 2 that a no-yield condition for F_s approximated by Eq. (18) is also a no-yield condition for the original F_s given by Eq. (6). The linearized yield condition $F_s \leq 0$ imposes p inequality constraints at any given point.

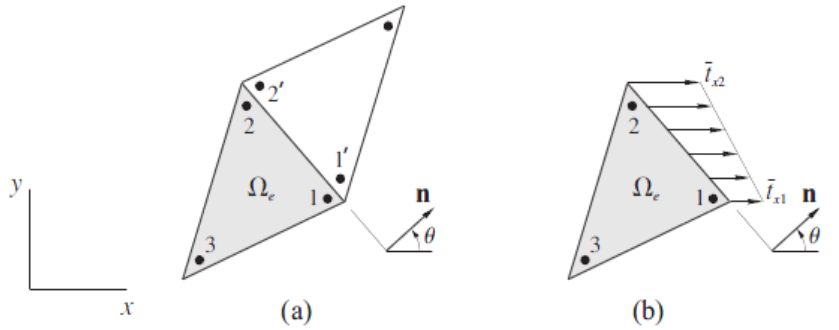

Figure 3. Lysmer finite element Ω_e has the edge 12: (a) in the interior of the body; (b) on the body boundary with prescribed traction (only the traction component $\bar{t}_x$ is shown)

Similarly, the failure criterion for the soil-reinforcement interface, given by the second of Eqs. (13), leads to two linear inequality constraints:

$$F_i = A_k\sigma_x + B_k\sigma_y + C_k\tau_{xy} - c_i \qquad k = p+1, p+2 \tag{20}$$

where

$$\begin{aligned} A_{p+1} &= \sin^2\theta\tan\phi_i - \tfrac{1}{2}\sin 2\theta & B_{p+1} &= \cos^2\theta\tan\phi_i + \tfrac{1}{2}\sin 2\theta \\ C_{p+1} &= -\sin 2\theta\tan\phi_i + \cos 2\theta & A_{p+2} &= \sin^2\theta\tan\phi_i + \tfrac{1}{2}\sin 2\theta \\ B_{p+2} &= \cos^2\theta\tan\phi_i - \tfrac{1}{2}\sin 2\theta & C_{p+2} &= -\sin 2\theta\tan\phi_i - \cos 2\theta. \end{aligned} \tag{21}$$

4 FINITE ELEMENT FORMULATION

We suppose that the soil mass is divided into a number of triangular elements and treated as an assembly of them. To apply the above equations to a finite element the definition of the boundary should be extended to include the traction continuity on the interelement portion Γ_i:

$$(\boldsymbol{t})^+ + (\boldsymbol{t})^- = \mathbf{0} \tag{22}$$

where the superscripts "+" and "−" denote the two sides of this boundary. In this section, the strong form of the equilibrium equation and mechanical boundary condition is used to derive Lysmer element, while a corresponding weak form is used to derive the other element.

4.1 Lysmer Finite Element

The macrostress field is linearly approximated over the Lysmer element Ω_e shown in Fig. 3 by

$$\boldsymbol{\sigma} = N_1\boldsymbol{\sigma}_1 + N_2\boldsymbol{\sigma}_2 + N_3\boldsymbol{\sigma}_3 \tag{23}$$

where

$$\boldsymbol{\sigma}_i = [\sigma_{xi} \quad \sigma_{yi} \quad \tau_{xyi}]^T \qquad N_i = \frac{1}{2A}(\alpha_i + \beta_i x + \gamma_i y) \qquad i = 1,2,3 \tag{24}$$

are the macrostress nodal values and the shape functions, respectively, with A standing for the triangle area. To evaluate

$$\alpha_i = x_j y_k - x_k y_j \qquad \beta_i = y_j - y_k \qquad \gamma_i = x_k - x_j \tag{25}$$

from the node coordinates, the indices i, j, k should be permuted in a natural order ($i \neq j \neq k$).

Substitution of Eq. (23) into Eq. (9) yields the discrete equilibrium equation

$$[\boldsymbol{L}_1 \quad \boldsymbol{L}_2 \quad \boldsymbol{L}_3] \begin{Bmatrix} \boldsymbol{\sigma}_1 \\ \boldsymbol{\sigma}_2 \\ \boldsymbol{\sigma}_3 \end{Bmatrix} = -\boldsymbol{b}, \tag{26}$$

where

$$L_i = \frac{1}{2A} \begin{bmatrix} y_j - y_k & 0 & x_k - x_j \\ 0 & x_k - x_j & y_j - y_k \end{bmatrix} \tag{27}$$

is defined by proper permutation of indices i, j, k. Eq. (9) is then satisfied pointwisely for a constant body force $\boldsymbol{b}$.

On the element edge which is in the interior of the soil (edge 12 shown in Fig. 3a), the traction $\boldsymbol{N\sigma}$ should be continuous. Since $\boldsymbol{\sigma}$ varies linearly within each element, continuity of $\boldsymbol{N\sigma}$ at the interelement nodes guarantees the continuity of $\boldsymbol{N\sigma}$ along the entire interelement boundary, which means, in fact, the enforcement of Eq. (22):

$$\left.\begin{matrix} \boldsymbol{N\sigma}|_{node\ 1} + \boldsymbol{N\sigma}|_{node\ 1'} = \boldsymbol{0} \\ \boldsymbol{N\sigma}|_{node\ 2} + \boldsymbol{N\sigma}|_{node\ 2'} = \boldsymbol{0} \end{matrix}\right\} \Rightarrow \begin{bmatrix} \boldsymbol{R} & \boldsymbol{0} & -\boldsymbol{R} & \boldsymbol{0} \\ \boldsymbol{0} & \boldsymbol{R} & \boldsymbol{0} & -\boldsymbol{R} \end{bmatrix} \begin{Bmatrix} \boldsymbol{\sigma_1} \\ \boldsymbol{\sigma_2} \\ \boldsymbol{\sigma_{1'}} \\ \boldsymbol{\sigma_{2'}} \end{Bmatrix} = \boldsymbol{0} \tag{28}$$

where

$$R = \begin{bmatrix} \cos\theta & 0 & \sin\theta \\ 0 & \sin\theta & \cos\theta \end{bmatrix}. \tag{29}$$

As the continuity of $\boldsymbol{N\sigma}$ across the edge does not mean continuity of $\boldsymbol{\sigma}$, the stress field generated by a mesh of Lysmer elements is discontinuous at the interfaces between elements.

On the element edge that falls on the body boundary with prescribed traction, the continuity of $\boldsymbol{N\sigma}$ should be replaced by the mechanical boundary condition given by Eq. (11). For the edge 12 shown in Fig. 3b, one writes

$$\begin{bmatrix} \boldsymbol{R} & \boldsymbol{0} \\ \boldsymbol{0} & \boldsymbol{R} \end{bmatrix} \begin{Bmatrix} \boldsymbol{\sigma}_1 \\ \boldsymbol{\sigma}_2 \end{Bmatrix} = \begin{Bmatrix} \bar{\boldsymbol{t}}_1 \\ \bar{\boldsymbol{t}}_2 \end{Bmatrix}. \tag{30}$$

The mechanical boundary condition is satisfied pointwisely if the components of $\bar{\boldsymbol{t}}$ vary linearly along the edge.

Unlike the usual form of the finite element method, each Lysmer element has its own nodes and several nodes in a mesh may share the same coordinates.

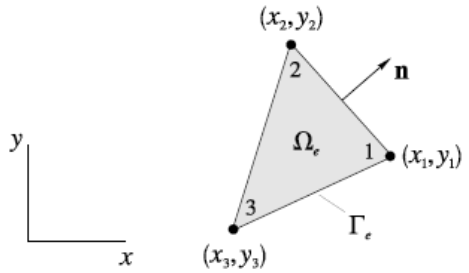

Figure 4. Weak equilibrium finite element Ω_e with the unit normal vector n on its boundary Γ_e

4.2 Weak Equilibrium Finite Element

Equation (9), Eq. (11) and Eq. (22) can be enforced to be satisfied on average over the triangular element of Fig. 4 by means of

$$\int_{\Omega_e} \boldsymbol{w}^T(\boldsymbol{D\sigma} + \boldsymbol{b})\, dx\, dy - \int_{\Gamma_t} \boldsymbol{w}^T(\boldsymbol{t} - \bar{\boldsymbol{t}})\, ds - \int_{\Gamma_i} \boldsymbol{w}^T \boldsymbol{t}\, ds = 0, \tag{31}$$

where $\boldsymbol{w} = \lfloor w_x \quad w_y \rfloor^T$ is an arbitrary weight function that is continuous across the element interfaces. The last integral, when considered jointly with those of the neighborhood elements, enforces Eq. (22).

In view of the divergence theorem

$$\int_{\Omega_e} \mathbf{w}^T(\mathbf{D\sigma})\, dx\, dy = \int_{\Gamma_e} \mathbf{w}^T \mathbf{t}\, ds - \int_{\Omega_e} (\mathbf{D}^T\mathbf{w})^T \boldsymbol{\sigma}\, dx\, dy, \tag{32}$$

Eq. (31) reduces to

$$\int_{\Gamma_u} \mathbf{w}^T \mathbf{t}\, ds + \int_{\Gamma_t} \mathbf{w}^T \bar{\mathbf{t}}\, ds + \int_{\Omega_e} \mathbf{w}^T \mathbf{b}\, dx\, dy - \int_{\Omega_e} (\mathbf{D}^T\mathbf{w})^T \boldsymbol{\sigma}\, dx\, dy = 0. \tag{33}$$

The portion Γ_u of the element boundary Γ_e falls on the soil boundary with prescribed displacement.

Substitution of Eq. (23) and the linearly varying weight function

$$\boldsymbol{w} = N_1\boldsymbol{w}_1 + N_2\boldsymbol{w}_2 + N_3\boldsymbol{w}_3, \tag{34}$$

with nodal values

$$\mathbf{w}_i = \lfloor w_{xi} \quad w_{yi} \rfloor^T \qquad i = 1, 2, 3, \tag{35}$$

into Eq. (33) yields

$$\begin{Bmatrix} \boldsymbol{w}_1 \\ \boldsymbol{w}_2 \\ \boldsymbol{w}_3 \end{Bmatrix}^T \left(\boldsymbol{F} - [\boldsymbol{G} \quad \boldsymbol{G} \quad \boldsymbol{G}] \begin{Bmatrix} \boldsymbol{\sigma}_1 \\ \boldsymbol{\sigma}_2 \\ \boldsymbol{\sigma}_3 \end{Bmatrix} \right) = 0 \tag{36}$$

where

$$\boldsymbol{G} = \frac{1}{6}\begin{bmatrix} y_2 - y_3 & 0 & x_3 - x_2 \\ 0 & x_3 - x_2 & y_2 - y_3 \\ y_3 - y_1 & 0 & x_1 - x_3 \\ 0 & x_1 - x_3 & y_3 - y_1 \\ y_1 - y_2 & 0 & x_2 - x_1 \\ 0 & x_2 - x_1 & y_1 - y_2 \end{bmatrix}$$

$$\mathbf{F} = \int_{\Gamma_t} [\boldsymbol{N}_1 \quad \boldsymbol{N}_2 \quad \boldsymbol{N}_3]^T \bar{\boldsymbol{t}}\, ds + \int_{\Omega_e} [\boldsymbol{N}_1 \quad \boldsymbol{N}_2 \quad \boldsymbol{N}_3]^T \boldsymbol{b}\, dx\, dy \tag{37}$$

and

$$\mathbf{N}_i = \begin{bmatrix} N_i & 0 \\ 0 & N_i \end{bmatrix}. \tag{38}$$

Since Eq. (36) holds for any arbitrary weight function, it follows that

$$[\boldsymbol{G} \quad \boldsymbol{G} \quad \boldsymbol{G}] \begin{Bmatrix} \boldsymbol{\sigma}_1 \\ \boldsymbol{\sigma}_2 \\ \boldsymbol{\sigma}_3 \end{Bmatrix} = \boldsymbol{F}. \tag{39}$$

The integral over Γ_u is zero because $\boldsymbol{w}$ will be chosen to be null over there in order to eliminate reaction force. The element enforces the equilibrium equation, given by Eq. (9), and the mechanical boundary condition, given by Eq. (11), to be satisfied by the discrete equation, given by Eq. (39), on average according to Eq. (33).

The conversion of the forces $\bar{\boldsymbol{t}}$ and $\boldsymbol{b}$ into the element nodal force $\boldsymbol{F}$ is identical to that for the well-known constant strain triangular (CST) element (Reddy, 2006). For a constant prescribed traction $\bar{\boldsymbol{t}} = \lfloor \bar{t}_x \quad \bar{t}_y \rfloor^T$ acting on an element edge of length *L*,

$$\int_{\Gamma_t} [\boldsymbol{N}_1 \quad \boldsymbol{N}_2 \quad \boldsymbol{N}_3]^T \bar{\boldsymbol{t}}\, ds = \frac{L}{2} \left\lfloor \bar{t}_x \quad \bar{t}_y \quad \bar{t}_x \quad \bar{t}_y \quad 0 \quad 0 \right\rfloor^T. \tag{40}$$

For a constant body force $\boldsymbol{b} = \lfloor b_x \quad b_y \rfloor^T$,

$$\int_{\Omega_e} [\boldsymbol{N}_1 \quad \boldsymbol{N}_2 \quad \boldsymbol{N}_3]^T \boldsymbol{b}\, dx\, dy = \frac{A}{3} \left\lfloor b_x \quad b_y \quad b_x \quad b_y \quad b_x \quad b_y \right\rfloor^T. \tag{41}$$

If $\boldsymbol{w}$ is viewed as the virtual displacement field, $\boldsymbol{D}^T\boldsymbol{w}$ is the virtual strain and Eq. (33) becomes the principle of virtual displacements adopted by Silva *et al.* (1999). The first formulation of the static theorem which satisfies the equilibrium equation and the mechanical boundary condition according to the principle of virtual displacements seems to have been proposed by Anderheggen and Knöpfel (1972). Their formulation was addressed to plate problems.

5 OPTIMIZATION PROBLEM

In the lower bound analysis, the equilibrium equation, the mechanical boundary condition and the yield criterion, expressed in terms of nodal stresses, are constraints of an optimization problem for the applied load maximization. The optimal solution

$$\lambda^* = \{\max \lambda \mid \boldsymbol{l}\bar{\boldsymbol{\sigma}} = \lambda \boldsymbol{f}_1 + \boldsymbol{f}_2,\ \boldsymbol{g_1}(\bar{\boldsymbol{\sigma}}, \bar{\boldsymbol{\sigma}}^r) \leq \mathbf{0},\ \boldsymbol{g_2}(\bar{\boldsymbol{\sigma}}) \leq \mathbf{0},\ \mathbf{0} \leq \bar{\boldsymbol{\sigma}}^r \leq \boldsymbol{\sigma}_o\} \tag{42}$$

identifies the collapse load, where the applied load has been splitted into two parts: $\lambda \boldsymbol{f}_1$ which is adjusted during the optimization by means of the load factor λ and $\boldsymbol{f}_2$ which is kept constant. The design variables are the nodal macrostresses $\bar{\boldsymbol{\sigma}}$ and reinforcement stresses $\bar{\boldsymbol{\sigma}}^r$.

The equality constraint

$$\boldsymbol{l}\bar{\boldsymbol{\sigma}} = \lambda \boldsymbol{f}_1 + \boldsymbol{f}_2 \tag{43}$$

arises from the assembly of Eq. (26), Eq. (28) and Eq. (30) for Lysmer finite elements, and from the assembly of Eq. (39) for weak equilibrium finite elements. The inequalities constraints

$$\boldsymbol{g_1}(\bar{\boldsymbol{\sigma}}, \bar{\boldsymbol{\sigma}}^r) \leq \mathbf{0} \qquad \boldsymbol{g_2}(\bar{\boldsymbol{\sigma}}) \leq \mathbf{0} \tag{44}$$

stem from the evaluation at each element node of the yield criteria, given by Eq. (18) and Eq. (20), and $\mathbf{0} \leq \bar{\boldsymbol{\sigma}}^r \leq \boldsymbol{\sigma}_o$ is the evaluation at each element node of the reinforcement stress. It can be demonstrated that enforcing the yield criteria at the element nodes is sufficient to satisfy them throughout the element.

For a given mesh, the weak equilibrium finite element leads to a much smaller problem size. The number of equality constraints is $2E + 4(I + B)$ for Lysmer formulation, where E is the number of elements, I is the number of interfaces between elements and B is the number of element loaded boundaries. The number of equality constraints is $2N$ for the weak equilibrium formulation, if the mesh has N nodes and the reduction due to the geometric boundary conditions is not taken into account. The numbers of inequality constraints and nodal stresses in one formulation may be quite different from the other. There will be $3(p + 2 + 2)E$ inequality constraints and $12E$ nodal stresses for Lysmer formulation, while these numbers reduce to $(p + 2 + 2)N$ inequality constraints and $4N$ nodal stresses for the weak equilibrium formulation.

The optimization problem solution is carried out following the steps: (a) formation of relevant quantities to set up the linear programming problem in MATLAB; (b) production of an MPS (Mathematical Programming System) file in MATLAB; (c) solution by FICO™ Xpress Optimization Suite, which contains a powerful LP optimizer composed by Newton Barrier, primal Simplex and dual Simplex methods.

6 NUMERICAL EXAMPLES

In this paper we consider two kinds of reinforced structures: strip footings (Fig. 5) and earth walls (Fig. 6), analyzed using the finite element meshes of Fig. 7 and Fig. 8, respectively, with $p = 200$.

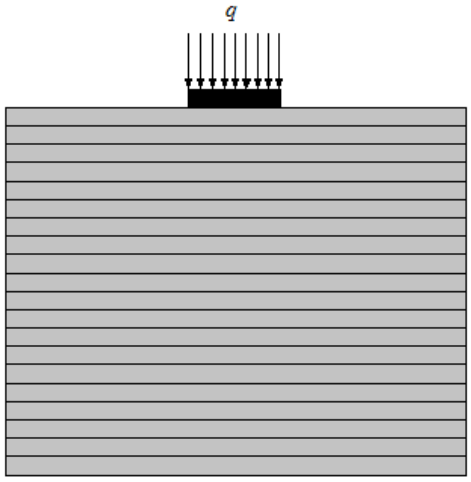

Figure 5. Strip footing with horizontal reinforcement

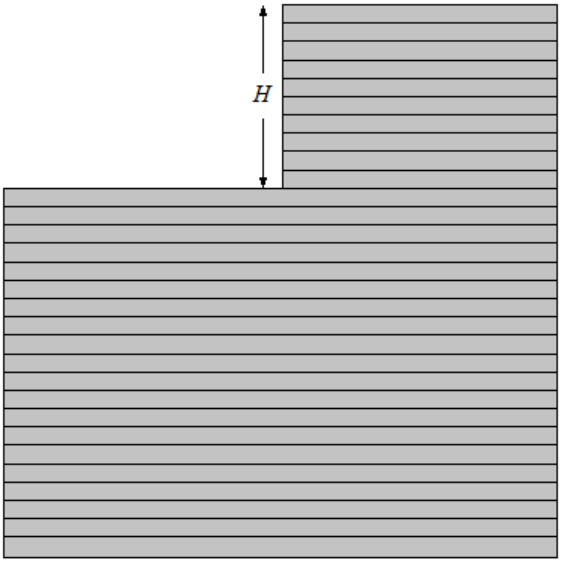

Figure 6. Earth wall with horizontal reinforcement

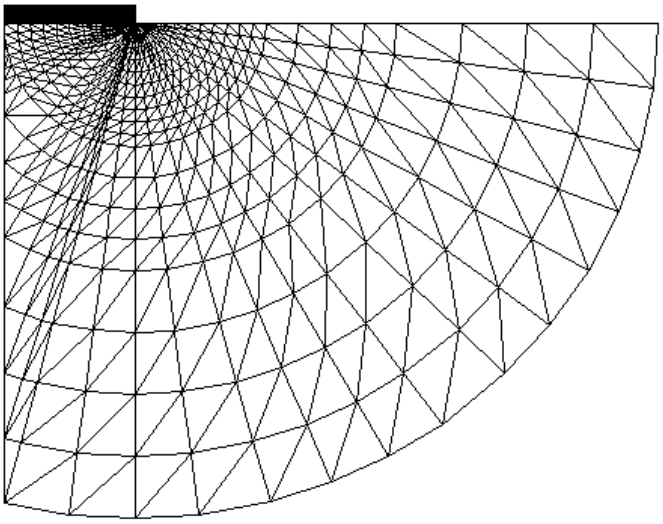

Figure 7. Strip footing mesh with 832 finite elements

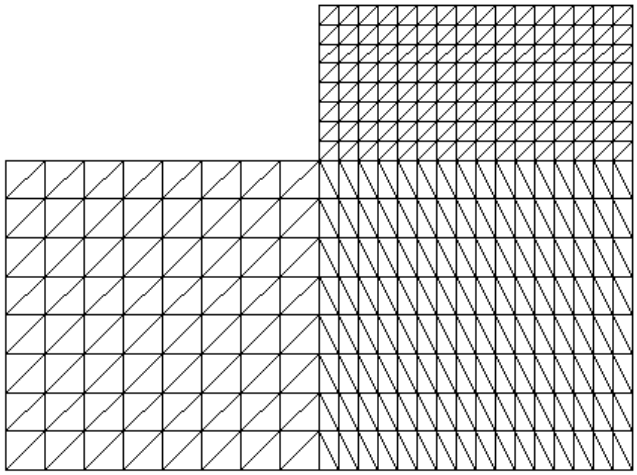

Figure 8. Earth wall mesh with 640 finite elements

6.1 Bearing capacity of a strip footing on cohesive-frictional reinforced soil

The advantages of having horizontal reinforcement on cohesive-frictional soils can be assessed by comparing the bearing capacities of reinforced and unreinforced soils. Figure 9 shows how the relative bearing capacities between reinforced and unreinforced soils vary with a dimensionless measure of the tensile strength of the reinforcement. Results are presented for friction angles of 10º, 20º and 30º and are derived from the weak equilibrium finite element with a perfect rough soil-reinforcement interface ($c_i = c, \phi_i = \phi$). As expected, for a given c the advantage of the reinforcement increases as the strength of the reinforcement is increased. Indeed, the bearing capacity ratio $q_{\text{reinforced}}/q_{\text{unreinforced}}$ increases almost linearly with the ratio σ_o/c. It is interesting to note, however, that the benefit from horizontal reinforcement is not strongly dependent on the soil angle of internal friction and is slightly less for soils with high angles of internal friction. At the scale of Fig. 9, results are indistinguishable for the weak equilibrium formulation and Lysmer's.

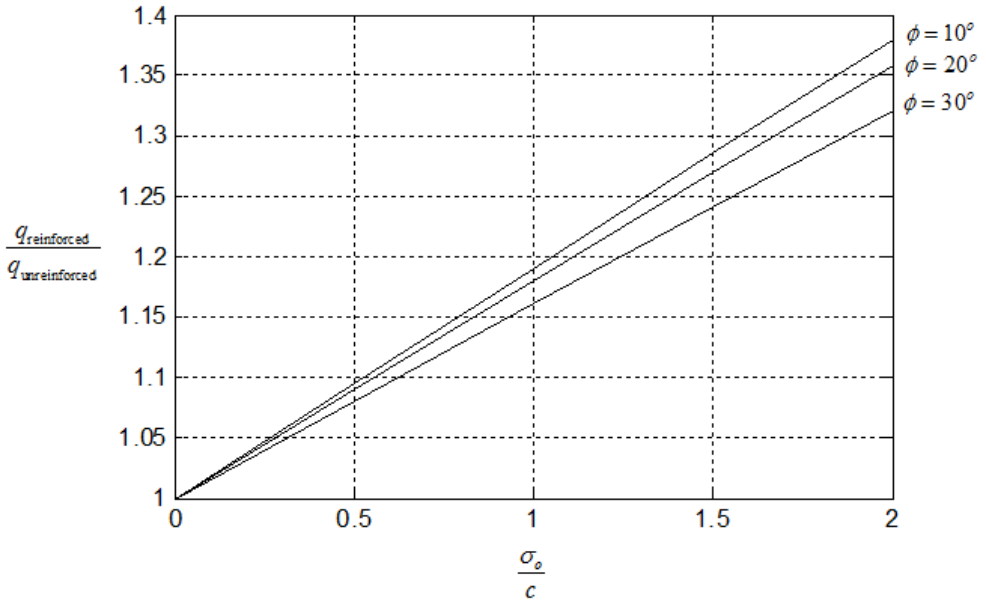

Figure 9. Effect of rough soil reinforcement ($c_i = c, \phi_i = \phi$) on bearing capacity for strip footing on cohesive-frictional soil with the weak equilibrium finite element

6.2 Stability of a cohesive-frictional reinforced wall

To assess the benefits of having horizontal reinforcement for cohesive-frictional walls, analyses were also performed for cases with and without reinforcement. The results are presented in Fig. 10 for the weak equilibrium finite element, where the ratio of the critical heights is plotted against a dimensionless measure of the tensile strength of the reinforcement. As expected, for a given c the critical height ratio $H_{\text{reinforced}}/H_{\text{unreinforced}}$ increases almost linearly with the measure of reinforcement strength σ_o/c. The results for three different fiction angles (10º, 20º and 30º) shown in Fig. 10 indicate that, unlike the footing problem discussed previously, the benefits of the horizontal reinforcement actually increase more significantly with the soil angle of internal friction. At the scale of Fig. 10, results are indistinguishable for the weak equilibrium formulation and Lysmer's.

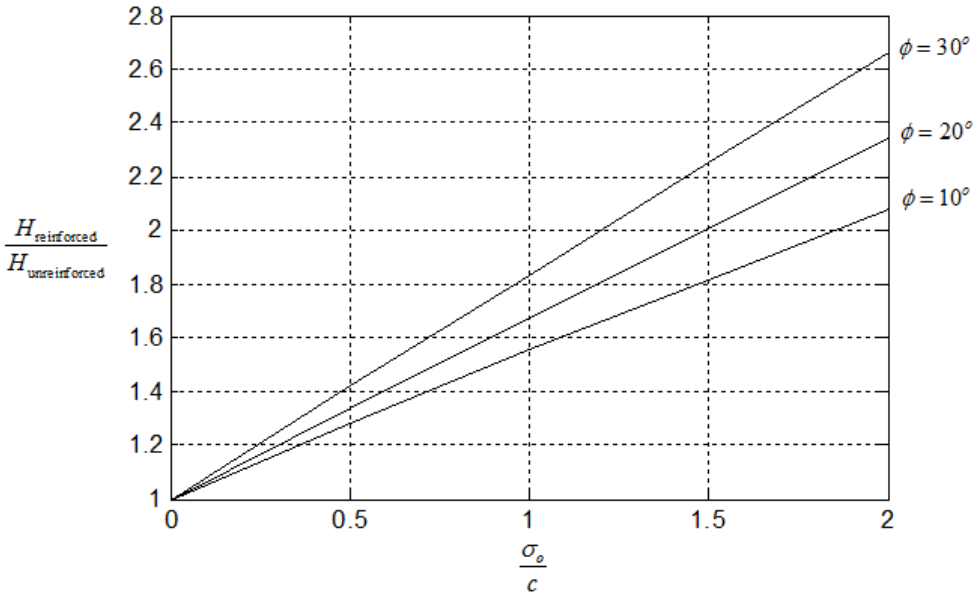

Figure 10. Effect of rough soil reinforcement ($c_i = c$, $\phi_i = \phi$) on height for retaining wall in cohesive-frictional soil with the weak equilibrium finite element

7 CONCLUSIONS

Two general finite elements based on the lower bound theorem has been presented for analysis of reinforced soil structures. We do not have knowledge of results in this field with the weak equilibrium finite element. The results with this triangular element and Lysmer's are quite similar for cohesive-frictional soil structures with a perfect rough soil reinforcement interface and the adopted meshes, although the number of equality and inequality constraints and the number of stress variables with the weak equilibrium formulation is much smaller than those with Lysmer formulation. In the case of the strip footing, for instance, the weak equilibrium formulation generates 846 equality constraints, 46,280 inequality constraints and 1,780 stress variables, while Lysmer formulation provides 6,684 equality constraints, 259,584 inequality constraints and 9,984 stress variables. It is believed that the combination of the weak equilibrium finite element with a powerful adaptive mesh generator can be an excellent tool for finite element limit analysis in this field.

REFERENCES

Anderheggen, E., Knöpfel, H., 1972. Finite element limit analysis using linear programming. *International Journal of Solids Structures*, vol. 8, n. 12, pp.1413–1431.

Chen, W.F., 1975. Limit Analysis and Soil Plasticity. Elsevier, Amsterdam.

de Buhan, P., Mangiavacchi, R., Nova, R., Pelligrini, G, & Salecon, J., 1989. Yield design of reinforced earth walls by a homogenization method. *Géotechnique*, vol. 39, n. 2, pp. 189–201.

de Buhan, P., & Siad, L., 1989. Influence of a soil-strip interface failure condition on the yield strength of reinforced earth. *Computers and Geotechnics*, vol. 7, n. ½, pp. 3–18.

FICO™ Xpress-Optimizer Reference Manual, Release 25.01. Fair Isaac Corporation, Birmingham, 2013.

Lysmer, J., 1970. Limit analysis of plane problems in soil mechanics. *Journal of the Soil Mechanics and Foundations Division*, 96, SM4, pp.1311–1334

MATLAB, 2015. www.mathworks.com.

Reddy, J.N., 2006. An Introduction to the Finite Element Method, 3rd ed., McGraw-Hill, New York.

Sawicki, A., 1983. Plastic limit behavior of reinforced earth. *Journal of Geotechnical Engineering*, vol. 109, n. 7, pp. 1000–1005.

Sawicki, A., 1988. Plastic behavior of reinforced earth. In Cheremisinoff, P. N., Cheremisinoff, N. P., & Cheng, S. L., eds, *Geotechnical Ocean Engineering*, vol. 3, chap. 3.

Silva, L.S., Farias, M.M., & Sahlit, C.L., 1999. Limit analysis in geotechnics using the finite element method and mathematical programming. *Proceedings of VII International Symposium on Numerical Models in Geomechanics*, Graz, pp. 215–220.

Yu, H.S., Sloan, S.W., 1997. Finite element limit analysis of reinforced soils. *Computers & Structures*, vol. 63, n. 3, pp. 567–577.